High Load Conditions Measured On A UH–60A In Maneuvering Flight

Robert M. Kufeld
Aerospace Engineer
NASA Ames Research Center
Moffett Field, California

and

William G. Bousman
Research Scientist
U.S. Army Aeroflightdynamics Directorate (ATCOM)
Moffett Field, California

Abstract

Maneuver data obtained under the NASA/Army UH–60A Airloads Program are examined qualitatively to show the effects of maneuvering flight conditions on rotor loads. Two test conditions have been selected for review based on a comparison of all 68 maneuvers conditions flown in the test program. These two conditions are ranked in the top ten for rotor load severity and show the effects of three-dimensional compressibility and dynamic stall on the rotor system. A detailed assessment of the section lift and moment calculated from measured pressures for each condition is provided.

Notation

$\frac{C_w}{\sigma} = \frac{GW}{\pi\sigma\rho\Omega^2R^4}$	gross weight coefficient
$M^2C_L = \frac{2L}{a^2\rho c}$	section normal force coefficient
$M^2C_M = \frac{2M_t}{a^2\rho c^2}$	section pitching moment coefficient
$M^2C_{pl} = \frac{2(p_l - p_\infty)}{a^2\rho c}$	lower surface pressure coefficient
$M^2C_{pu} = \frac{2(p_u - p_\infty)}{a^2\rho c}$	upper surface pressure coefficient
a	speed of sound, ft/sec
b	number of blades
c	blade chord, ft
GW	aircraft gross weight, lbs
g	acceleration due to gravity
L	section normal force, lbs/in
M	local Mach number
M_t	sect. pitching moment, in-lb/in
n_z	load factor, g
P	pitch-link force, lbs
p	surface pressure, lbs/in^2
p_∞	static pressure, lbs/in^2
R	blade radius, ft
μ	advance ratio
ρ	air density, slug/ft^3
σ	rotor solidity, $bc/\pi R$
Ω	rotor rotational speed, rad/sec
ψ	rotor azimuth, deg

Presented at the American Helicopter Society 51th Annual Forum, Fort Worth, TX, May 9-11, 1995.

Introduction

The load amplification effects of maneuvering flight on rotor and control loads are well known throughout the helicopter industry. It is this loading, particularly for military aircraft, that the designer must consider when sizing rotor parts for strength. However, present analyses are not able to accurately predict rotor loads during maneuvers and, therefore, designers must use prior flight test data as a basis for design. To obtain improved analytical models it is important to investigate maneuvering flight conditions so as to improve our understanding of the loading phenomena.

Little flight test data with both rotor airloads and structural loads are available for maneuver flight conditions. Beno[1] presented data from one condition in 1973 for a CH–53A and Kufeld, Cross, and Bousman[2] showed three conditions from the UH–60A Airloads Program[3]. Since the publication of Ref. 2 additional UH–60A maneuver test conditions have been flown and added to the data base. These additional maneuvers show rotor and control system loading significantly greater than previously reported.

The present paper will briefly discuss the maneuver flying that was performed with the UH–60A during the test program and will relate these maneuvers to operational requirements. Methods used to examine maneuver severity will be discussed and the maneuvers will be ranked accordingly. Two of the most severe maneuvers will be examined in detail and the aerodynamic sources of the loads will be discussed.

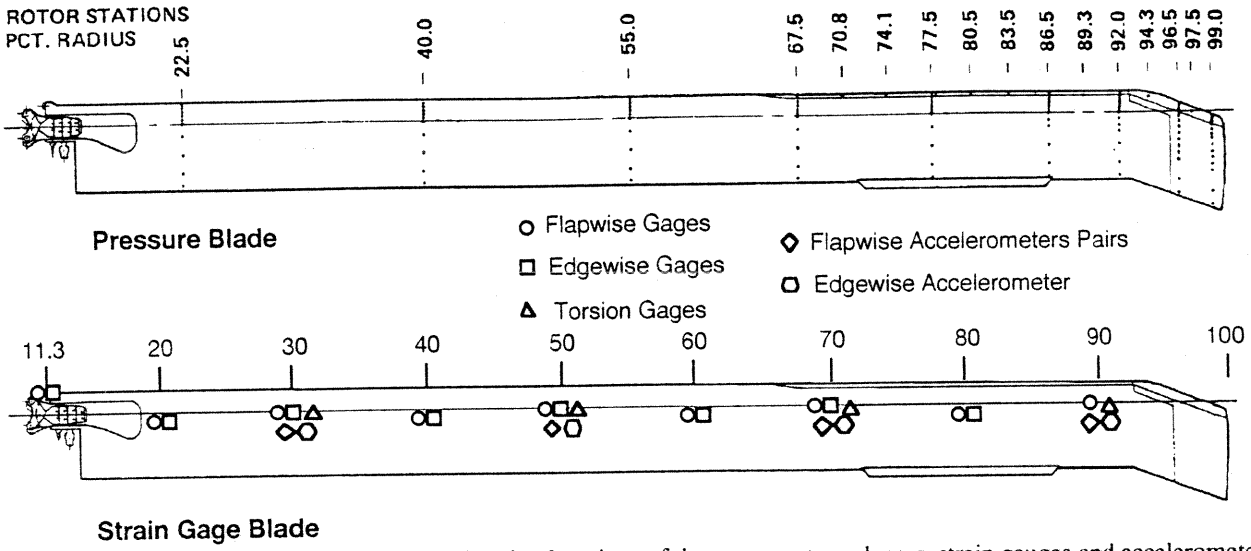

Figure 1. UH-60A instrumented blades showing locations of the pressure transducers, strain gauges and accelerometers.

Flight Test Data

Highly-instrumented blades were designed, built, and installed on a standard UH-60A aircraft[3,4] as shown in Fig. 1. One blade had a total of 221 pressure transducers installed in nine spanwise arrays plus an additional 21 pressure transducers installed near the leading edge between the spanwise arrays. A second blade was instrumented with strain gauges and accelerometers to measure the blade structural loads and response. The aircraft was also instrumented to measure the vehicle state and numerous other parameters[3].

The rotor blade data were sampled and digitized in the rotating system and a PCM stream was fed down though a slip ring at a data rate of approximately 7.5 Mbits/sec. The pressure data were sampled at 2142 Hz which corresponds to approximately 500 samples/revolution. However, anti-aliasing filters were set at about 500 Hz so that the effective bandwidth corresponded to about 120 harmonics. Structural data were recorded at a lower rate which corresponded to an effective bandwidth of about 24 harmonics.

68 test points (counters) obtained during the UH–60A Airloads Program are classified as maneuvers. This set includes all of the classical maneuvers used during aircraft development such as symmetric pull-ups and pushovers, rolling pullouts, roll reversals, and diving turns. The 68 maneuver cases are shown in Fig. 2 in terms of load factor and airspeed and compared to the UH–60A structural envelope. In some maneuvers, both maximum and minimum extrema in load factor were obtained, hence more than one point is included for these maneuvers.

To evaluate the severity of the Airloads maneuvers flown, load factor data obtained during free engagement air-to-air combat flights with the UH–60A during the Air-to-Air Combat Test (AACT) flying[5] are also shown in Fig. 2. Solid circles are for UH–60A/OH–58A engagements and solid squares for UH–60A/AH-76 engagements. Open square symbols represent maneuvers examined in this paper. In general, significantly higher positive load factors were recorded during the air-to-air combat tests, but at lower speeds. The maneuvers flown during the UH–60A Airloads

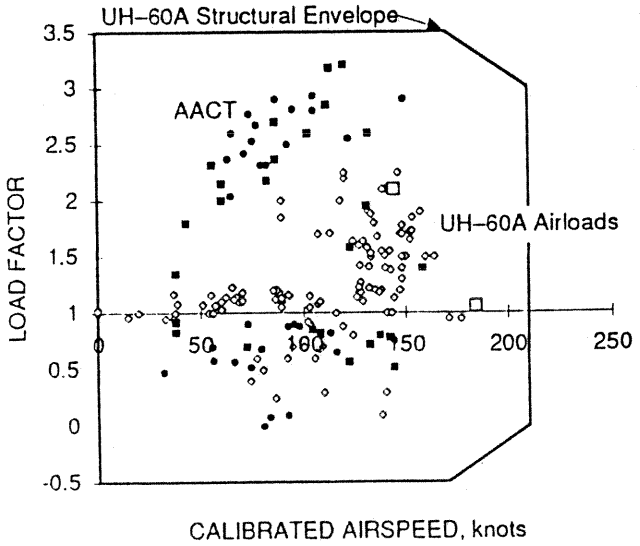

Figure 2. Load factor/airspeed diagram for UH–60A Airloads Program maneuvers (open symbols) and AACT maneuvers (solid symbols).

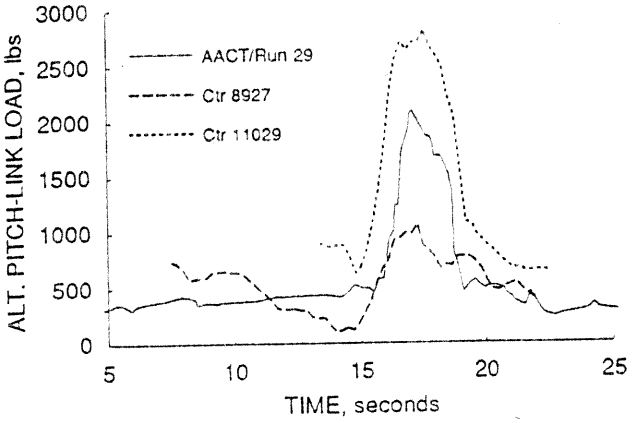

Figure 3. Comparison of alternating pitch-link loads for three maneuvers.

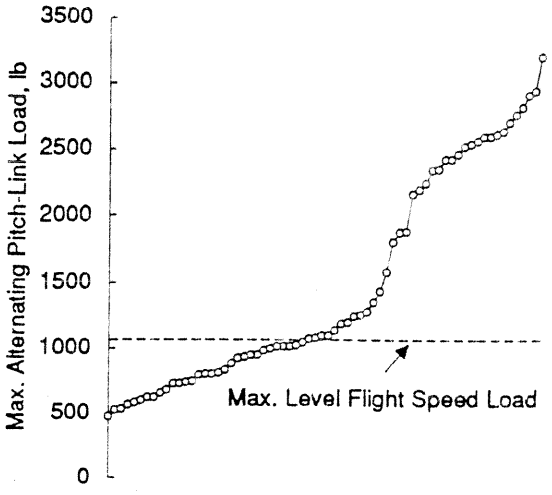

Figure 4. Rank order of pitch-link loads for airloads maneuvers

Program show a reduced test envelope compared to the operational experience as reflected in the AACT data. However, this conclusion needs to be qualified as the effects of airspeed on the structural loads developed in maneuver are, perhaps, more important than load factor. Fig. 3, for example, compares a "typical high control load maneuver" from Ref. 5 with two maneuvers from the airloads program. The AACT maneuver achieves 2.45g at about 123 knots and the resulting alternating pitch-link loads are about 2100 lb. A lower speed pull-up[2] results in a maximum load factor of 2.06g at 100 knots and only 1100 lbs for the alternating pitch-link loads. However, a pull-up based on the original UTTAS maneuver of the UH–60A design specification reaches 2.12g at 139 knots and, as a consequence of the higher speed, causes the alternating pitch-link loads to exceed 2800 lb. This alternating load is as high as any reported in Ref. 5, and indicates that the present data base loading conditions exceed, in general, loads encountered in operational use.

The 68 maneuvers were examined within the TRENDS data base[6] and the maximum alternating loads encountered during each maneuver were extracted for 36 different structural parameters, including blade flap and chord bending moments, torsion moments, pitch-link loads, damper force, blade flapping, shaft bending and torque, and hub vertical acceleration. These loads were then sorted within a spreadsheet to order the maneuvers by the size of the alternating loads for each measurement. An example of this procedure is shown in Fig. 4 where the alternating pitch-link load for blade 1 is plotted in rank order with the most benign maneuver on the left and the most severe on the right. For reference, the alternating pitch-link load at the maximum airspeed in level flight is also shown in the figure. This figure indicates that approximately half of the 68 maneuvers resulted in loads that were more severe than those encountered in level flight at the maximum level flight speed.

To identify the most severe maneuvers based on the rank ordering process, only six of the 36 structural measurements were used: pitch-link load, torsion moment at 0.30R, blade flap bending moment at 0.113R and 0.60R, and blade chord bending moment at 0.113R and 0.60R. The ten most severe maneuvers for each of six structural measurements were selected to form a subset of 24 maneuvers. A scoring system was then used to rank these 24 maneuvers and the resulting ten most severe are shown in Table 1 along with their rank order for each of the six measurements. Note that the most severe maneuver, a diving right turn at 140 knots (Counter 11680), shows the highest loads for the pitch-link force, the torsion moment, and the root chord bending, but was only the fifteenth most severe maneuver based on flap root bending. This suggests the importance of looking at a variety of maneuvers to understand the phenomena that are included.

Four of the ten maneuvers in Table 1 are plotted in Fig. 5 and compared to the matrix of steady, level flight test points obtained in the UH–60A Airloads Program[7] and to an aerodynamic rotor lift boundary obtained in wind tunnel testing of a model rotor by McHugh[8]. The level flight points are shown by the solid square symbols and the McHugh boundary by the solid line. For Counters 11029, 11679, and 11680 the open points represent the mean value of $n_Z(C_W/\sigma)$ and μ during each rotor revolution. Counter 11029, the UTTAS pull-up, represents a dynamic maneuver and the effective weight coefficient, $n_Z(C_W/\sigma)$, increases rapidly from about 0.08 at maneuver initiation to a peak of almost 0.17. The diving turns, Counters 11679 and 11680, were intended to be steady test points but, as can be seen in Fig. 5, it was difficult to maintain constant load factor during these highly banked, high-speed turns with rates of descent of 4000 and 5400 ft/min respectively. The fourth

Table 1. UH–60A flight test most severe maneuvers.

		RANK ORDER					
MANEUVER	COUNTER	PITCH-LINK LOAD	TORSION MOMENT r/R=0.30	FLAP BENDING r/R=0.113	FLAP BENDING r/R=0.60	CHORD BENDING r/R=0.113	CHORD BENDING r/R=0.60
RT TURN, 140 KIAS, 60° AOB	11680	1	1	15	4	1	14
UTTAS PULL-UP, 130 KIAS, 2.1G	11029	3	8	1	15	8	4
RT TURN, 140 KIAS, 55° AOB	11679	2	2	23	7	23	15
DIVE ROLL PULLOUT, 120 KIAS	11028	6	5	8	23	3	22
PULL-UP, 120 KIAS, 2.25G	11023	10	7	2	26	4	25
LT TURN, 130 KIAS, 60° AOB	11686	9	3	7	17	12	5
DESCENT, 186 KIAS (VNE)	11682	24	24	28	1	21	2
LT TURN, 120 KIAS 60° AOB	11660	8	4	13	14	7	6
RT TURN, 130 KIAS, 60° AOB	11672	13	6	10	18	5	8
UTTAS PULL-UP, 130 KIAS, 1.8G	11031	4	14	5	13	11	9

maneuver is the maximum dive speed point, Counter 11682, and this maneuver was reasonably steady. Intermediate steady diving flight conditions are shown in this figure with open circles.

Counters 11029, 11679, and 11680, as shown in Fig. 5, extend well beyond the McHugh lift boundary and it may be anticipated that the resulting severe loads are a consequence of dynamic stall. Counter 11682, on the other hand, is within the rotor thrust boundary and it is expected that the loads in this case are caused by compressibility effects. For the purposes of this paper, two maneuvers will be investigated – the UTTAS pull-up, Counter 11029 and the maximum dive speed case, Counter 11682.

UTTAS Maneuver

The UTTAS maneuver was one of the specification requirements for the Utility Tactical Transport Aerial System (UTTAS) program that led to the development of the UH–60A Black Hawk aircraft in the early 1970s. The maneuver is entered at the maximum level flight speed of the aircraft and the nose is pitched up so that a 1.75g normal acceleration or load factor is developed and held for at least three seconds without losing more than 30 knots of airspeed. The maneuver differs from the conventional symmetric pull-up in that the maneuver entry is from a level flight attitude rather than in a dive. This maneuver, although originally based on the need for terrain avoidance, is also typical of free engagement, air-to-air combat flying as shown in flight tests of the UH–60A performed under the U.S. Army's Air-to-Air Combat Test program[5]. However, in air-to-air combat flying, the entry speed is normally well below the maximum level flight speed required by the UTTAS maneuver.

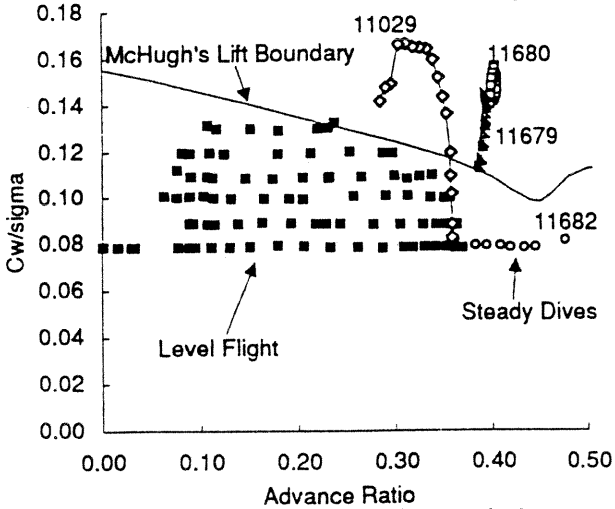

Figure 5. Comparison of rotor thrust and advance ratio for UH–60A maneuvers and level flight conditions.

Two UTTAS maneuvers were flown with the UH–60A during the maneuver phase of the flight test program: a pull-up to 1.8g (Counter 11031) and 2.1g (Counter 11029). The latter maneuver is examined in detail here. This second UTTAS maneuver was one of the most severe flown during the entire program and, although a peak load factor of 2.1g was achieved, the original specification requirement was not met in that a 1.75g load factor was held for only 2.5 seconds. Fig. 6 shows the time history of the maneuver based on rotor revolutions. The normal load factor, pitch rate, and airspeed shown are the mean values for each revolution, while the alternating pitch-link load is the peak alternating load recorded in each revolution. A revolution requires approximately 0.23 seconds for the UH–60A.

The peak pitch rate occurs from Revs 11 to 15 and varies from 14.2 to 14.7 deg/sec. The peak load factor occurs a second or so later, from Revs 14 to 18, and varies from 2.08 to 2.12 g. The maximum alternating pitch-link load lags the load factor by approximately a revolution and varies from 2640 to 2820 lbs. During this period, from Revs 11 to 19, the advance ratio drops from 0.349 to 0.296. Despite the rapidity of this maneuver, in human terms, the duration of the peak loading occurs over four or five revolutions and may be considered relatively steady.

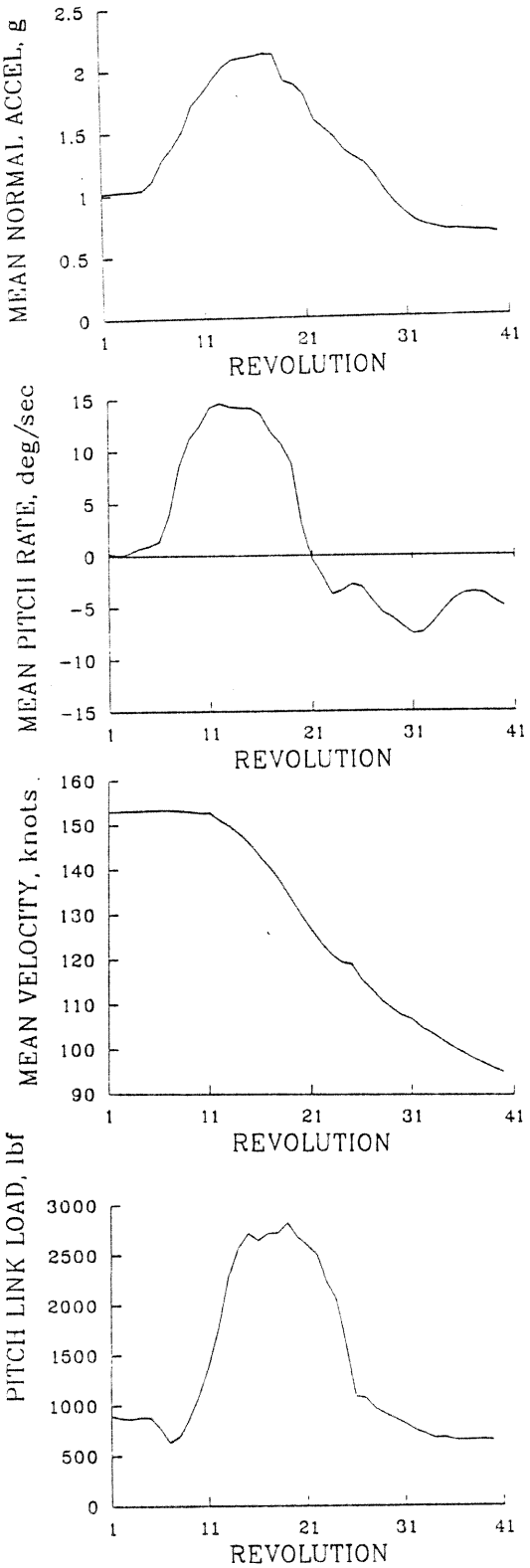

Figure 6. UH–60A a) mean load factor, b) mean pitch rate, c) mean velocity and d) alternating pitch-link load during the UTTAS pull-up.

The blade pitch-link loads are examined over the duration of the maneuver in Fig. 7. Each revolution of the maneuver is placed adjacent to the next revolution to create a surface plot that shows the pitch-link load behavior during the maneuver. The pitch-link load character is similar during the entry and exit period of the maneuver, showing the large positive to negative load on the advancing side of the disk that is typical of high-speed level flight[2,9]. During the highest load factor portion of the maneuver the character of the loading changes noticeably, with an increase in the alternating load as well as a higher frequency content. The increased loading is a consequence of dynamic stall on the blade as shown in Fig. 8, where the section pitching moment, M^2C_M, at 0.865R is shown as a function of blade azimuth and revolution count. In this figure, the section moment is shown with the negative moment above the zero

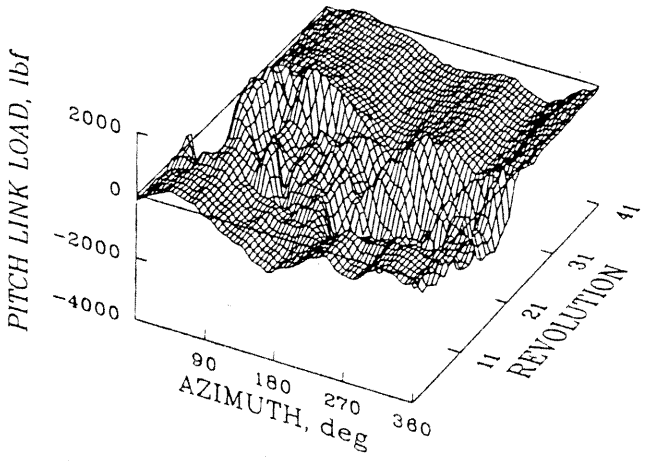

Figure 7. Pitch-link load as a function of azimuth and rotor revolution during UTTAS pull-up; 0 to 24 harmonics.

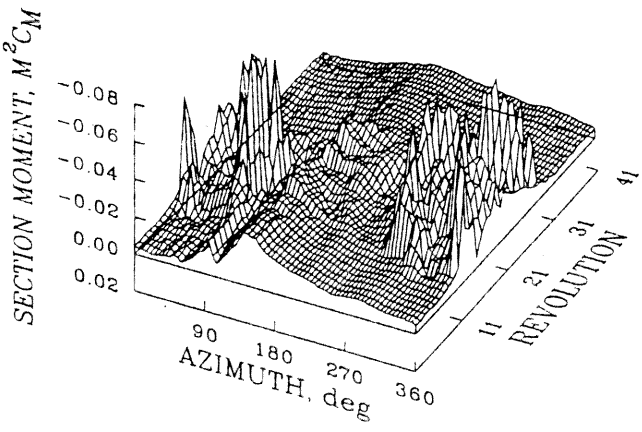

Figure 8. Section moment at r/R = 0.865 as a function of azimuth and rotor revolution during UTTAS pull-up; 0 to 120 harmonics.

plane which is contrary to normal convention. Again, as with Fig. 7, the section moment over the entry and exit portions of the maneuver is typical of high-speed level flight. At about Rev 09 a fairly sudden break in the pitching moment is seen at about 295 deg and, over the next two revolutions, this break moves forward to about 260 deg and the negative peak in the section moment at this radial station is seen at about 270 deg. A second stall cycle develops with a negative peak at about 335 deg and, a revolution or two later, a third stall cycle is seen, now in the first quadrant, at about 55 deg.

The development of the three dynamic stall cycles at 0.865R is shown in more detail in Fig. 9, which uses a sliding vertical scale for each successive rotor revolution. The initiation of the first dynamic stall cycle is clearly seen in the fourth quadrant and, as the aircraft load factor increases, this first cycle moves progressively into and towards the front of the third quadrant as the second and third cycles develop. Once the peak load factor is achieved the cycle essentially reverses.

The development of the dynamic stall cycles on the rotor is also seen in the control system loads as shown in Fig. 10. A positive pitch-link load (tension), as shown in this figure, is equivalent to a positive section moment on the blade. The three cycles of dynamic stall observed in Fig. 9 are also seen in Fig. 10. The dynamics of the blade motion, here indicated by the pitch-link force, are intimately related to the aerodynamics of the dynamic stall cycles. There is no direct measurement of the angular displacement at the radial station where the pressure measurements are obtained and the estimation of these displacements based on torsional moments, pitch-link loads, and blade root feathering is a formidable task. The frequency spectrum of the torsion moment at 0.30R shows non-integer responses at 4.85/rev and 5.85/rev and it is believed that these frequencies represent the first two blade torsion/control system modes.

The section moment distribution along the blade for Rev 17, one of the most highly loaded revolutions, is shown in Fig. 11 and the distribution of normal force is shown in Fig. 12. Inboard on the blade, at 0.225R and 0.40R, dynamic stall occurs almost directly over the nose of the aircraft. The dynamic stall in this case is most likely caused by angle-of-attack changes induced by the flow over the fuselage and is not seen in level flight prior to the maneuver. Further outboard, at 0.675R, a normal force (Fig. 12) increase and reduction is seen in the first quadrant that is associated with the third dynamic stall cycle but less of an effect is seen for the first and second cycles. The section moment, in particular, shows little variation at this radial station. Outboard on the blade the three dynamic stall cycles are clearly seen for both the pitching moment and normal force distributions, except, perhaps, at the blade tip.

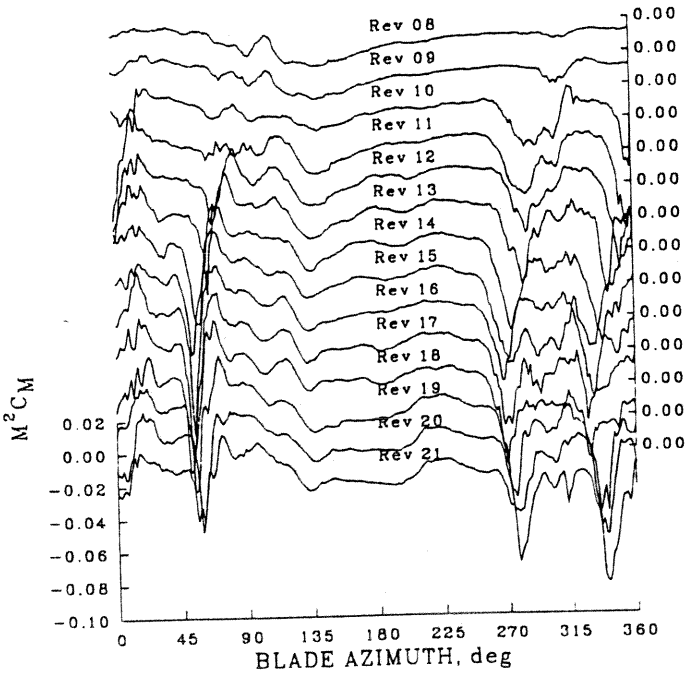

Figure 9. Offset plot of section moment at r/R = 0.865 as a function of azimuth and rotor rev during UTTAS pull-up; 0 to 120 harmonics.

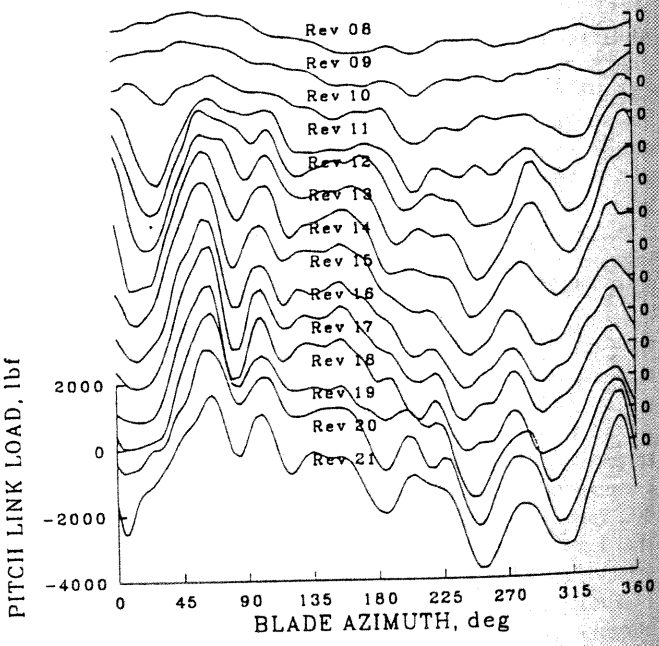

Figure 10. Offset plot of pitch-link load as a function of azimuth and rotor rev during UTTAS pull-up; 0 to 24 harmonics.

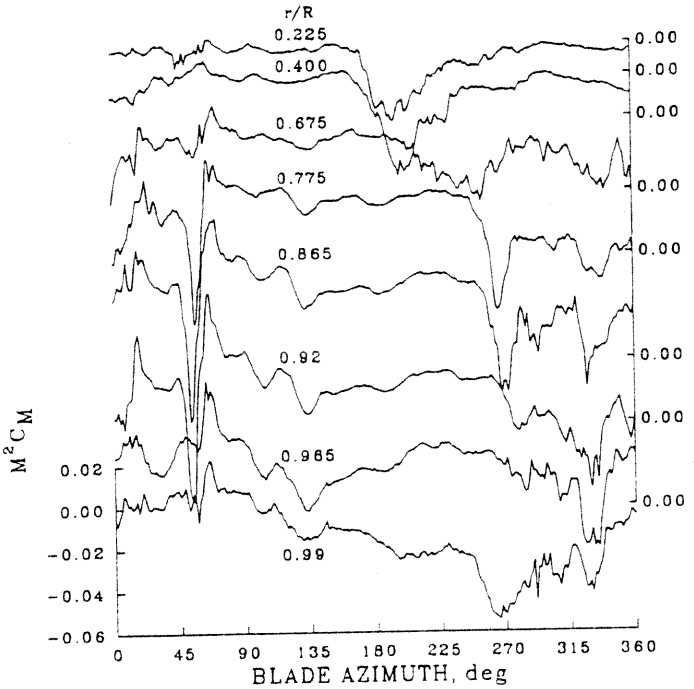

Figure 11. Offset plot of blade section moment as a function of rotor azimuth and blade radius for Rev 17 of UTTAS pull-up maneuver; 0 to 120 harmonics.

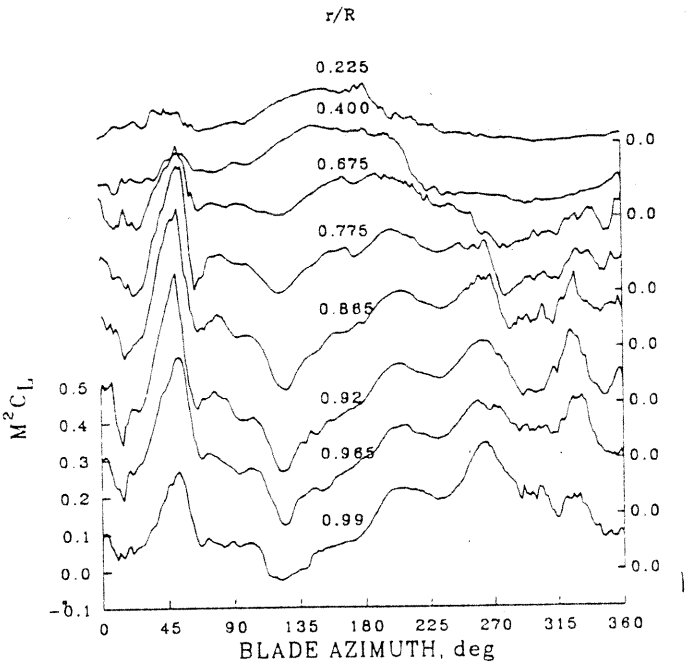

Figure 12. Offset plot of blade section normal force as a function of rotor azimuth and blade radius for Rev 17 of UTTAS pull-up maneuver; 0 to 120 harmonics.

The strongest pitching moment changes caused by dynamic stall are seen at 0.775R and 0.865R. The upper surface pressures at 0.865R are shown in Fig. 13 for Rev 17 and provide insight into the blade aerodynamics during this maneuver. The initial pressure collapse is seen at 0.030c at about 245 deg and by 0.049c or 0.080c the lift increase induced by the vortex shed in the dynamic stall cycle is clearly seen. The passage of the shed vortex is evident in the pressure variation at each chord station and the vortex leaves the trailing edge just past 270 deg. Interestingly, the flow is supercritical over the front of the airfoil just prior to the shedding event and this can be more clearly seen in Fig. 14 where the offset has been removed and the surface pressure corresponding to M = 1 has been added to show the boundary of the supercritical flow field. This supercritical flow is seen to develop from 0.030c to 0.080c just past 180 deg. At about 205 deg the extent of the supercritical flow is reduced and a shock is seen moving forward over the transducer at 0.080c. The shock continues to move forward, crossing the transducer at 0.049c at about 225 deg. The pressure collapse and vortex shedding then occurs at about 245 deg and the flow momentarily becomes supercritical at 0.010c This may be related to the vortex shedding event.

The flow is quite unsteady following the first dynamic stall cycle as shown in Fig. 13 and may not completely reattach prior to the shedding of a second dynamic stall vortex at about 315 deg. This second vortex convects along the airfoil surface and passes over the trailing edge at about 335 deg, although this is not so readily seen as in the first

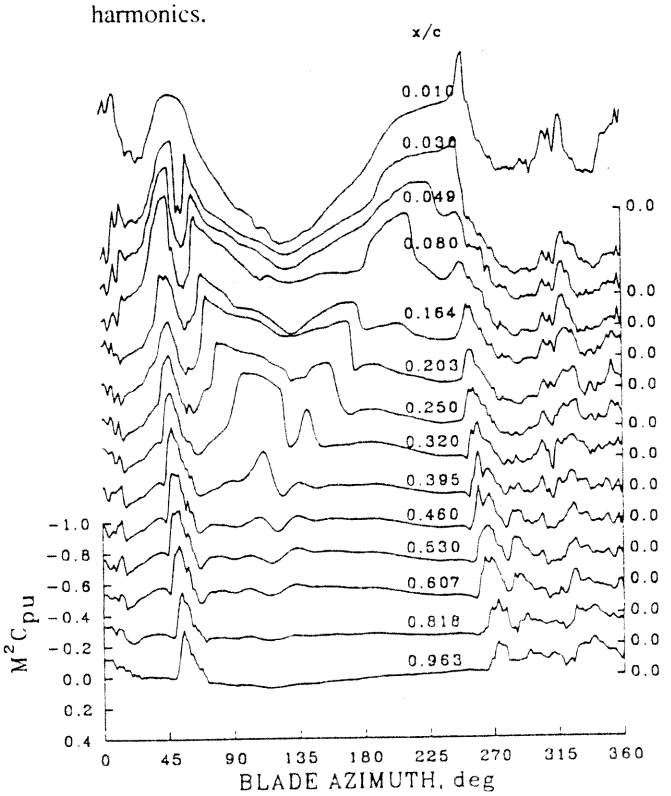

Figure 13. Offset plot of upper surface pressure coefficients at r/R = 0.865 as a function of rotor azimuth and blade chord for Rev 17 of UTTAS pull-up maneuver; 0 to 120 harmonics.

cycle. The 0.010c transducer shows another peak at about 10 deg, but this does not appear to develop into a full-strength vortex and the section pitching moment does not show signs of an associated stall peak. The third dynamic stall cycle is characterized by strong supercritical flows and an interacting dynamic stall vortex as can be seen in both Figs. 13 and 14. At about 25 deg the flow becomes supercritical over the front of the airfoil. At about 45 deg a vortex is apparently shed and the pressure shows a sharp reduction as the vortex-induced velocity reduces the local velocity. This effect continues well back on the airfoil, although by the time the vortex reaches mid-chord the flow is subcritical and the pressure peak that is observed is directly induced by the vortex passage. The vortex passage is complete by 55 deg and the event has occurred much more quickly than on the retreating side.

The blade pressure distribution inboard on the blade where dynamic stall is forced by the fuselage-induced changes in angle of attack is also of interest. Fig. 15 shows the upper surface pressures at 0.40R for Rev 17 of the maneuver. A region of supercritical flow is seen over the transducer at 0.010c in the first quadrant but not further back on the airfoil. Then, in the second quadrant, supercritical flows are observed at 0.010c and 0.049c as the angle of attack increases as the blade approaches the nose of the aircraft. At about 160 deg there is a rapid drop in the pressure at these locations and a shed vortex is apparent that passes the trailing edge at about 225 deg.

Near the blade tip the aerodynamics associated with the three dynamic stall cycles are different than that observed

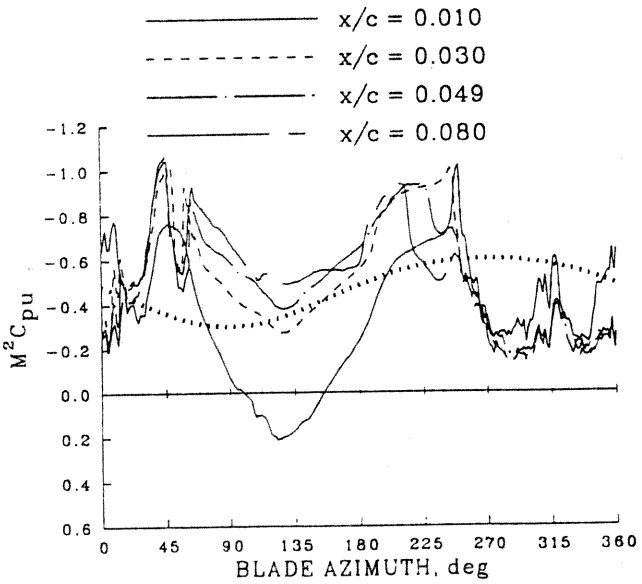

Figure 14. Upper surface pressure coefficients at r/R = 0.865 as a function of rotor azimuth for Rev 17 of UTTAS pull-up maneuver; 0 to 120 harmonics, pressure corresponding to M = 1 indicated by heavy dashed line.

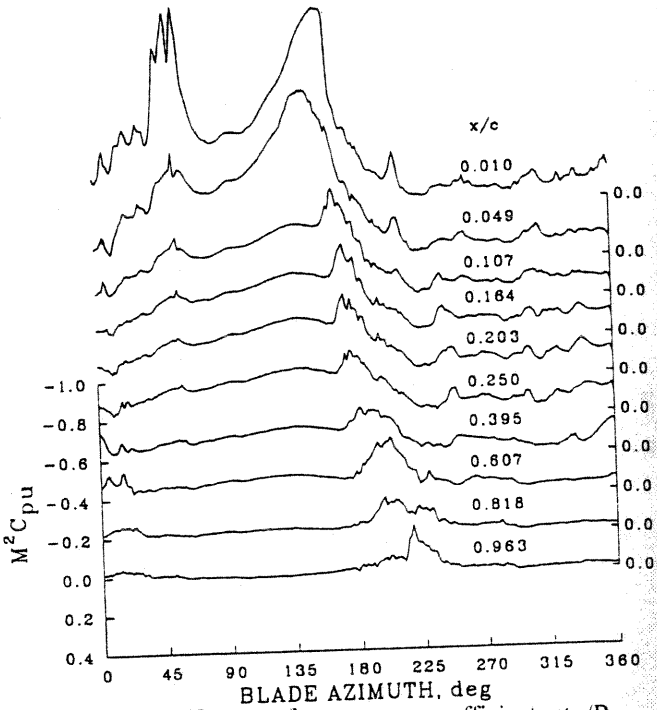

Figure 15. Upper surface pressure coefficients at r/R = 0.40 as a function of rotor azimuth and blade chord for Rev 17 of UTTAS pull-up maneuver; 0 to 120 harmonics.

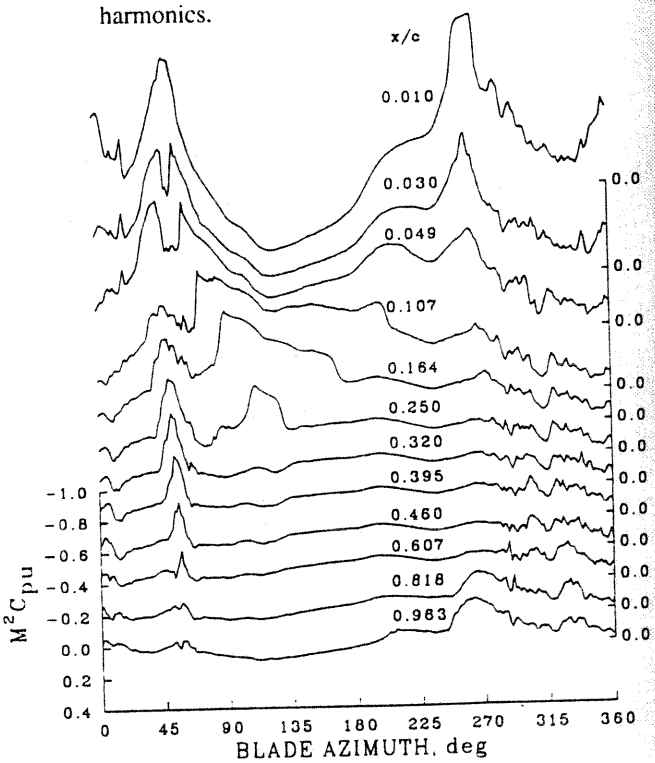

Figure 16. Upper surface pressure coefficients at r/R = 0.99 as a function of rotor azimuth and blade chord for Rev 17 of UTTAS pull-up maneuver; 0 to 120 harmonics.

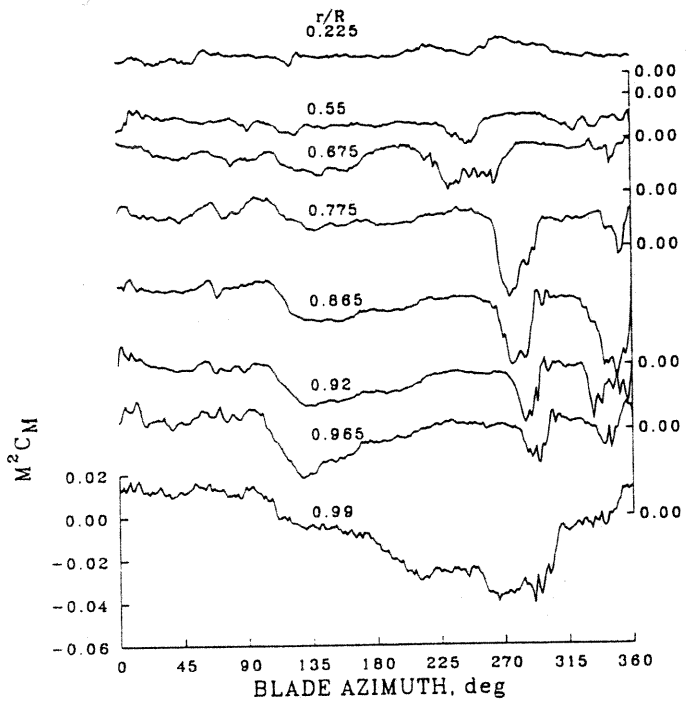

Figure 17. Offset plot of blade section moment for level flight, $\mu = 0.236$, $C_W/\sigma = 0.1335$ as a function of rotor azimuth and blade radius; 0 to 120 harmonics.

inboard. Fig. 16 shows the upper surface pressures at 0.99R for Rev 17 of the UTTAS maneuver. An area of supercritical flow is observed near 270 deg for the 0.010c and 0.030c transducers but there is no clear vortex shedding from the leading edge. However, there is a pressure rise at the last two stations at about this azimuth that may indicate local separation in this region and is likely the primary cause for the negative moment observed in Fig. 11. For the second stall cycle, at about 335 deg, again there is little sign of a dynamic stall vortex except possibly over the aft section of the airfoil, for the 0.607c through 0.963c transducers. However, the section moment as shown in Fig. 11 does suggest that the dynamic stall vortex seen on the inboard sections of the blade does extend to the tip, at least in a weakened state. Fig. 16 shows that on the advancing side of the rotor supercritical flows are apparent over the first 25% of the airfoil, but these are not quite so extensive as at 0.865R because of tip relief. Separation of a leading edge vortex appears to occur for the third dynamic stall cycle, but the vortex-induced changes in pressure die out rapidly and do not appear over the aft section of the airfoil and, therefore, a large section moment is not observed at this station (r/R = 0.99).

Dynamic stall in level flight[7] shows many similarities to the severe maneuver examined here. Fig. 17 shows the section moment distribution for Counter 9017, which is the highest loading condition obtained in steady flight during the UH–60A Airloads Program. Two dynamic stall cycles are seen for this level flight condition outboard of 0.675R, rather than three, but these two cycles appear similar in behavior to the first two cycles described for Counter 11029 (Fig. 11). It is likely that analytical models that can correctly predict the dynamic stall behavior in level flight will also be able to predict the dynamic stall characteristics in maneuvers. However, key to any prediction will be the correct modeling of the control system and blade torsional flexibilities as the oscillatory nature of the dynamic stall cycles is closely tied into the oscillations in the torsional degree of freedom.

Maximum Dive Speed

The "DESCENT, 186 KIAS (VNE)" test point, Counter 11682, is a steady, high-speed dive at the maximum design speed of the UH–60A, $\mu \sim 0.48$. Data were recorded in unaccelerated flight with rotor thrust near that of the maximum level flight speed data. The airload data shown here were taken from one rotor revolution during the "maneuver" as all revolutions for this steady condition were similar.

The maximum dive speed condition, as shown in Table 1, exhibited the highest alternating loads for mid-span flap and chord bending moments. Fig. 18 shows the increase in the alternating flap bending moments at three radial stations as a function of advance ratio. Beyond maximum level flight speed, $\mu \sim 0.37$, the data are for dive conditions with the dive angle increasing to 14 deg at the maximum dive speed case. In general, once past the speed for minimum power the alternating moments increase with advance ratio in a monotonic fashion and, in this respect, this maneuver is quite different from the UTTAS maneuver where the loading behavior changes abruptly at the inception of dynamic stall.

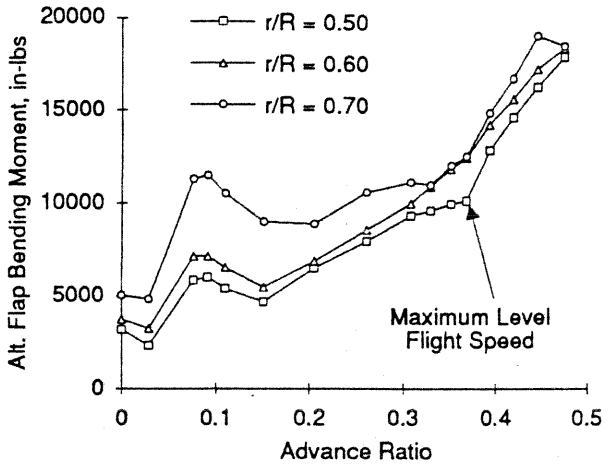

Figure 18. Mid-span blade flap bending loads as a function of advance ratio.

The radial distribution of normal force for the maximum dive speed is shown in Fig. 19 and the distribution of pitching moment in Fig. 20. Inboard on the blade, Fig. 19 shows that the lift is greatest in the second quadrant and over the nose of the aircraft and this greater lift may be caused, in part, by fuselage-induced flow. Areas of reversed flow are seen in the third and fourth quadrants at the two inboard stations as expected for this advance ratio. Outboard on the blade small regions of negative lift develop at 0.675R and 0.775R at about 90 deg. This area of negative lift becomes larger, both in azimuthal extent and peak negative load, on the outer portion of the blade from 0.865R to 0.965R.

The section pitching moments, Fig. 20, show large positive values inboard on the blade in the reversed flow region. Outboard on the blade one to three oscillatory cycles are seen on the advancing side, but little evidence of dynamic stall is observed on the retreating side except for an incipient stall cycle that starts at about 305 deg at 0.92R.

The distribution of surface pressure at 0.92R for Counter 11682 is shown in Fig. 21 for the upper surface and Fig. 22 for the lower surface. The most noticeable features in the upper surface distributions in Fig. 21 are the development of shocks and regions of supercritical flow on the advancing side and an incipient dynamic stall cycle in the fourth quadrant. Supercritical flow develops over the front of the airfoil in the first quadrant and the expansion of this flow rearward is traced by the passage of the shock that is associated with this supercritical flow. The shock is clearly seen at 0.080c at about 25 deg and as it moves rearward on the airfoil it strengthens. At about 65 deg, at 0.607c, the shock appears to be slowing as the Mach number approaches its maximum value, but the supercritical flow region does extend back past 0.818c between 110 and 135 deg. The region of supercritical flow and the associated shock then moves forward as the Mach number is reduced and the shock or its interaction with the boundary layer can be seen to nearly 180 deg.

Dynamic stall is observed in the fourth quadrant as shown by the upper surface pressures in Fig. 21. The leading edge pressure collapses at about 290 deg and a dynamic stall vortex is apparent by the time it moves rearward to 0.080c. No trailing edge separation is observed for this case and, by analogy to the dynamic stall development described for the UTTAS maneuver, this represents an incipient dynamic stall condition. A second dynamic stall cycle may also be occurring at the beginning of the first quadrant, but no influence of the vortex is seen beyond the quarter chord.

The lower surface pressures at 0.92R are shown in Fig. 22. As the lift becomes negative near the end of the first quadrant, supercritical flow develops over the front of the airfoil and a strong shock appears and moves aft extending as far back as 0.607c. Then, in the second quadrant, as the lift becomes positive again, the shock moves rapidly to the

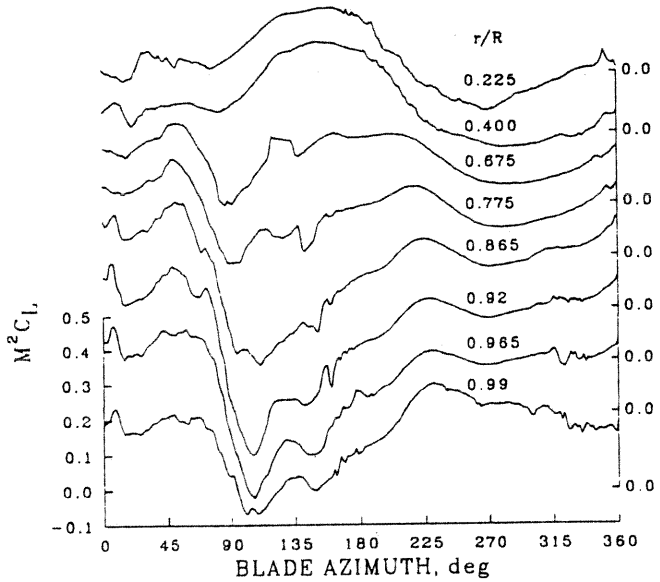

Figure 19. Offset plot of blade section normal force as a function of rotor azimuth and blade radius for maximum dive speed maneuver; 0 to 120 harmonics.

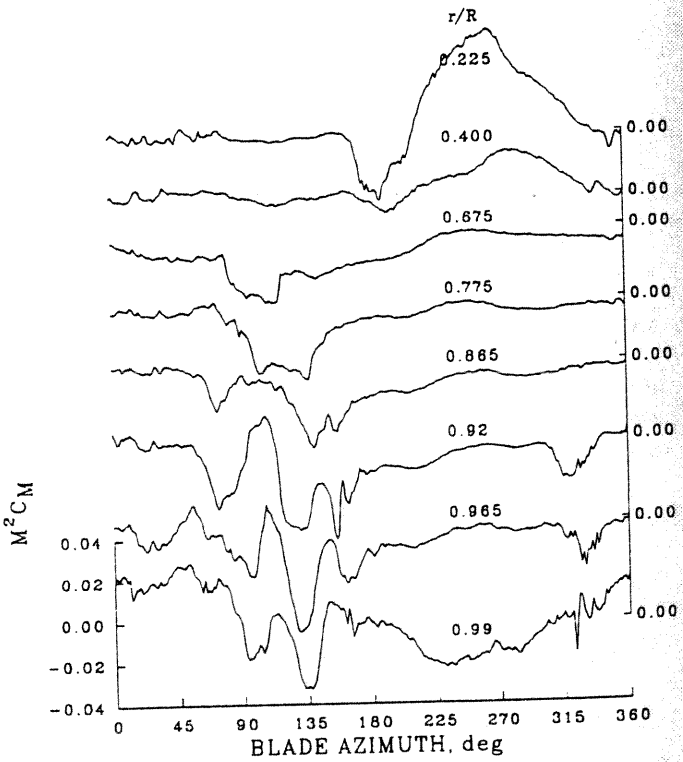

Figure 20. Offset plot of blade section moment as a function of rotor azimuth and blade radius for maximum dive speed maneuver; 0 to 120 harmonics.

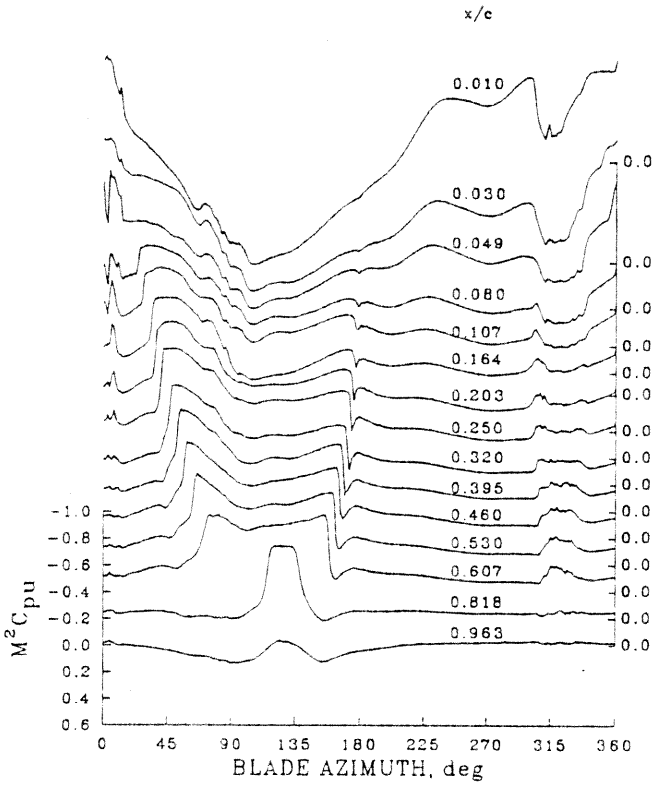

Figure 21. Offset plot of upper surface pressure coefficient as a function of rotor azimuth and blade chord, r/R = 0.92; 0 to 120 harmonics.

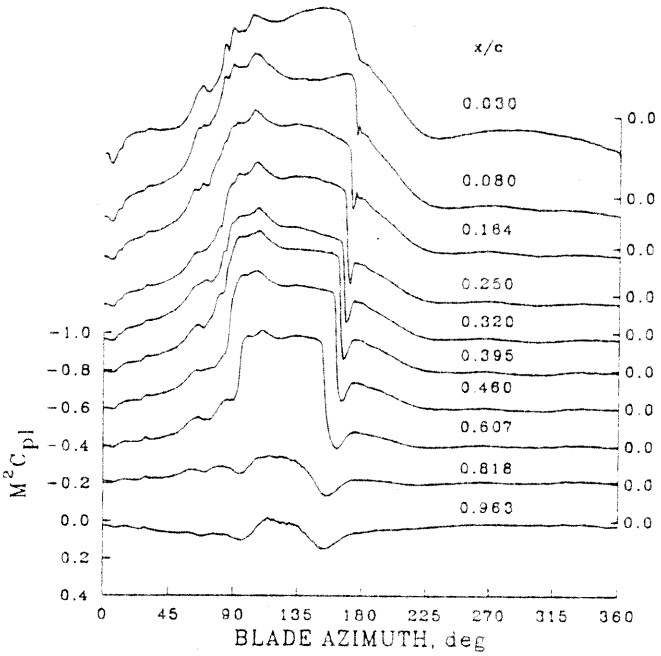

Figure 22. Offset plot of lower surface pressure coefficient as a function of rotor azimuth and blade chord, r/R = 0.92; 0 to 120 harmonics.

front of the airfoil as the supercritical region shrinks and disappears. The development of the supercritical regions on the upper and lower surfaces as shown in Figs. 21 and 22 results in high section loads. Because the supercritical flow on the lower surface forms later than on the upper surface there is an initial increase in normal force created by the upper surface supercritical flow and a decrease in section moment because of the rearward shift in the pressure distribution. As the supercritical flow develops on the lower surface this process is reversed and the normal force becomes negative and the moment more positive. As the supercritical flow regions move forward in the second quadrant they are slightly out of phase and this may explain the rapid lift and moment variations observed in Figs. 19 and 20.

The development of the normal force and pitching moment as airspeed is increased is shown in Figs. 23 and 24 at the 0.92R location. The upper curve in each figure is the maximum level flight speed and the subsequent curves are for progressively steeper dive conditions ending with the maximum dive speed condition. All of the lift distributions at 0.92R in Fig. 23 show the region of negative lift in the second quadrant that is required to maintain rotor trim. As airspeed is increased the negative lift increases and the rate of change of lift also increases, but the fundamental character of the data does not change. The alternating flap bending moments also increase over this airspeed range, as shown in Fig. 18, but in a monotonic fashion and, it appears, the section normal force increases in the same fashion. Contrary to the UTTAS maneuver, discussed earlier, there is no triggering event which shows a change in the character of the loads and a substantial increase in their size.

The section pitching moment data, in Fig. 24, show qualitative changes as the aircraft goes to increasingly higher speeds. A substantial oscillation develops at the end of the first quadrant by $\mu = 0.40$ and this oscillation becomes substantially larger as speed is increased. As discussed above, this advancing side change in pitching moment is believed to result from two factors: the movement of the supercritical flow regions further aft on the airfoil at higher Mach numbers and the difference in phase between the supercritical flow regions on the upper and lower surfaces. This qualitative change in character and increase in loads is a triggering event that is analogous to dynamic stall as discussed for the UTTAS maneuver. However, the resulting loads are not as serve as in the dynamic stall case (see Table 1) and, therefore, this case is not a limiting condition for the torsion and control system loads.

Conclusions

Maneuver conditions in the UH–60A Airloads Program data base have been examined to identify those maneuvers which are most severe in terms of structural loading. In general, the highest loads are seen for high load factor or

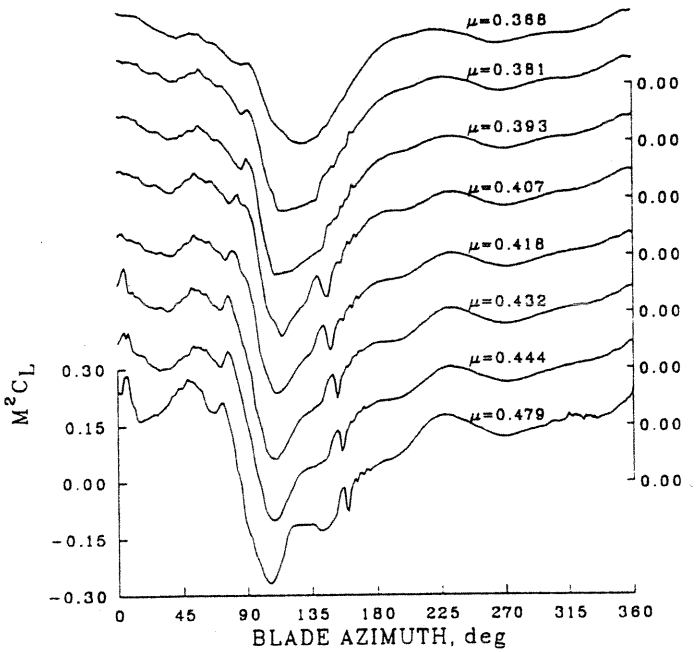

Figure 23. Offset plot of section normal force at radial station r/R = 0.92 as a function of rotor azimuth and advance ratio (from maximum level flight speed to maximum dive speed); 0 to 120 harmonics.

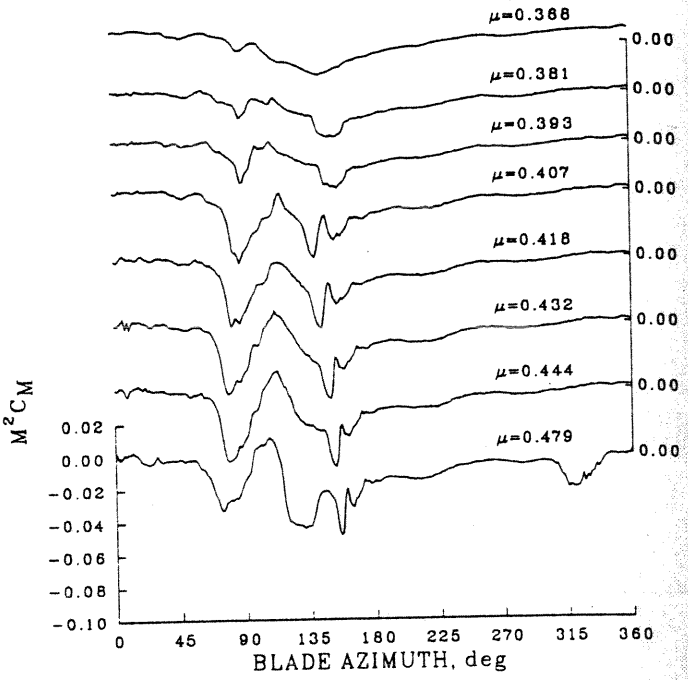

Figure 24. Offset plot of section moment at radial station r/R = 0.92 as a function of rotor azimuth and advance ratio (from maximum level flight speed to maximum dive speed); 0 to 120 harmonics.

high speed conditions or some combination of both. Based on a ranking of the maneuvers for various structural components, two maneuvers were selected for a detailed examination of the aerodynamic loading. The first maneuver, a UTTAS pull-up to 2.1g (Counter 11029) resulted in some of the largest pitch-link loads encountered in the flight test program. From an examination of the aerodynamic loads it is apparent that these high loads are a consequence of dynamic stall that occurs on the outboard portion of the blade and this dynamic stall behavior is intimately related to the control system and blade torsional flexibility. The second maneuver, a steady condition at the aircraft maximum dive speed (Counter 11682) showed the largest midspan blade loads measured in the program. An examination of this case shows that the bending moments and the airloads both increase with airspeed in a monotonic fashion and that there is no triggering event or phenomena that is responsible for the high loads.

References

1. Beno, E.A., "Analysis of Helicopter Maneuver-Loads and Rotor-Loads Flight Test Data", NASA CR-2225, March, 1973.

2. Kufeld, R.M., Cross, J.L., and Bousman, W.G., "A Survey of Rotor Loads Distribution in Maneuvering Flight," American Helicopter Society Aeromechanics Specialists Conference Proceedings, San Francisco, CA, January 1994.

3. Kufeld, R.M., Balough, D.L., Cross, J.L., Studebaker, K.F., Jennison, C.D., and Bousman, W. G., "Flight Testing of the UH–60A Airloads Aircraft", 50th Annual American Helicopter Society Forum, Washington, DC., May 1994.

4. Kufeld, R.M. and Loschke, P., "UH–60 Airloads Program: Status and Plans," AIAA Aircraft Design, Systems, and Operations Meeting, Baltimore, MD, September 1991.

5. Washuta, K.W. and Stocker, B.P., "Air-to-Air Combat Test (AACT II) Maneuvering Flight Loads for UH–60A and AUH–76 Helicopters," USAAVSCOM TR–86–D–1, April 1986.

6. Bondi, M J. and Bjorkman, W.S., "TRENDS: A Flight Test Relational Database User's Guide and Reference Manual," NASA TM 108806, June 1994.

7. Coleman, C.P. and Bousman, W.G., "Aerodynamic Limitations of the UH–60A Rotor", American Helicopter Society Aeromechanics Specialists Conference Proceeding,, San Francisco, CA, January 1994.

8. McHugh, F.J., "What Are the Lift and Propulsive Force Limits at High Speed for the Conventional Rotor?," American Helicopter Society 34th Annual Forum, Washington, D.C., May, 1978.

9. Maier, T.H., and Bousman, W.G., "An Examination of the Aerodynamic Moment on Rotor Blade Tips Using Flight Test Data and Analysis," Eighteenth European Rotorcraft Forum, Avignon, France, September 1992.